

ARTICLE TEMPLATE

**MIQCP and MISOCP-Based Solution Methods
for the Multi-Layer Thin Films Problem**

Deniz Tuncer and Burak Kocuk

Faculty of Engineering and Natural Sciences, Sabanci University, Istanbul, Turkey 34956

ARTICLE HISTORY

Compiled January 22, 2026

ABSTRACT

The Multi-Layer Thin Films Problem is a materials science problem that aims to enhance the reflectance of a metallic substrate by designing multi-layer coatings composed of different dielectric materials and thicknesses. While previous studies on the problem mostly rely on heuristic approaches and are designed for single wavelength applications, this work addresses the problem using global optimization techniques for multiple wavelengths. We develop an exact nonconvex mixed-integer quadratically constrained programming (MIQCP) model to solve this problem. We also develop a mixed-integer second-order cone programming relaxation that has computational advantage over the MIQCP model. Our numerical experiments yield solutions that have average reflectance of 99% over the visible spectrum (380–770 nm) and 95% over the broad spectrum (300–3000 nm).

KEYWORDS

global optimization; mixed-integer linear programming; mixed-integer quadratic programming; applications in materials science

1. Introduction

Reflectance is an electromagnetic property of materials that quantifies the percentage of incident light energy reflected by the material. In some optics applications such as telescope and laser systems, materials with high reflectance are preferred. The Multi-Layer Thin Films Problem involves a metallic surface whose reflectance is to be enhanced by coating it with thin layers of various dielectric materials.

The Multi-Layer Thin Films Problem can be considered a special case of the optimization problems of the following form (Kocuk 2022):

$$\max_{T_1, \dots, T_N, w} f(w) \quad (1a)$$

$$\text{s.t. } pT_1T_2 \cdots T_N = w, \quad (1b)$$

$$T_1, \dots, T_N \in \mathcal{T} \quad (1c)$$

In Problem (1), $p \in \mathbb{C}^{r \times d}$ is a given matrix that represents the initial state, $f : \mathbb{C}^{r \times d} \rightarrow \mathbb{R}$ is a real-valued function, and $\mathcal{T} \subseteq \mathbb{C}^{d \times d}$ is a given set of matrices. Also, $w \in \mathbb{C}^{r \times d}$ represents the final state, after N many matrices are multiplied with p . Since constraint (1b) involves multiplication of matrix variables, this is a nonlinear

CONTACT Deniz Tuncer. Email: dtuncer@sabanciuniv.edu

CONTACT Burak Kocuk. Email: burak.kocuk@sabanciuniv.edu

optimization problem. This problem setting, also called switched linear systems (Wu and He 2020), represents a system whose initial state is p , and the system evolves through each decision, T_1, \dots, T_N . Then, the performance of the final state w of the system is evaluated by the function f . Despite its seemingly simple structure, even a special case of this problem, where f is linear and \mathcal{T} is a finite set, is shown to be NP-Hard (Tran and Yang 2017). In the context of the Multi-Layer Thin Films Problem, the variables T_1, \dots, T_N denote the transfer matrices corresponding to the selected coating material and thickness for layer n , f is the reflectance function that will be introduced in Section 2 and p is the 2×2 identity matrix.

A review of the literature reveals that the design of multi-layer thin films are typically guided by heuristic methods (Larruquert and Keski-Kuha 1999; Dobrowolski et al. 2002; Hobson and Baldwin 2004; Shi et al. 2017; Keçebaş and Şendur 2018). One of the earliest studies on the Multi-Layer Thin Films Problem is Turner and Baumeister (1966), where the authors define the problem and come up with a heuristic idea: stacking alternating layers of high and low refractive-index materials yield good reflectance values. In the literature, there are numerous studies that utilize this idea (see Southwell (1980); Popov et al. (1997); Keçebaş and Şendur (2018)). Another commonly used heuristic relies on the idea of selecting the coating thicknesses as optical thickness of a quarter wavelength (see Macleod (2010)). A special heuristic method called needle optimization is first coined by Tikhonravov, Trubetskoy, and DeBell (1996) for this problem, and is utilized by Mashaly (2024) for a practical energy saving application. In general, heuristics are utilized in the inverse design process, which involves choosing a coating, computing its reflectance and then adjusting the thicknesses (e.g., So and Rho (2019)). Particle swarm optimization and numerical optimization methods are also used in a similar manner to come up with coating designs (Kim, Kaya, and Hajimirza 2021; Zhang et al. 2024). Recent advances in deep learning technologies have facilitated its application to the design of multi-layer thin films as well (Jiang, Osamu, and Chen 2020; Fouchier et al. 2021).

While heuristic methods may work well for some specific wavelengths, they achieve it with high number of layers. We suggest that optimization techniques have significant potential for achieving improved reflectance while coating with fewer layers, which may decrease the likelihood of implementation errors. To the best of our knowledge, the studies Azunre et al. (2019); Wu and He (2020); Kocuk (2022) represent the attempts to address this problem using mathematical optimization methods. In Kocuk (2022), the author formulates and solves a nonconvex mixed-integer quadratically constrained program (MIQCP) for increasing the reflectance of the substrate for light coming at only a single wavelength.

In this study, our objective is to maximize the average reflectance of the substrate over a range of wavelengths. In other words, our proposed designs will be robust to changes in the wavelength of the incoming light. We aim to achieve these robust designs using global optimization methods, whose utilization in this domain is limited. Our contributions are as follows: We propose a novel MIQCP-based global optimization method for the Multi-Layer Thin Films Problem that aims to maximize the average reflectance over a spectrum of wavelengths. We also devise a convex mixed-integer relaxation of the MIQCP in the form of a mixed-integer second-order cone program (MISOCP). We compare our results with a heuristic from the literature and find out that our methods are able to provide better solutions that yield higher reflectance values with fewer coating layers.

Our paper is organized as follows: In Section 2, we introduce some concepts related to the underlying optics concepts and then provide an optimization formulation. In

Section 3, we propose our MIQCP and MISOCP-based methods. In Section 4, we present our computational results. Lastly, in Section 5, we discuss our key findings and the future work that may follow.

2. Optimization Formulation

Developing an optimization formulation for the Multi-Layer Thin Films Problem requires some background information on the optical properties of the materials. Therefore, before we provide a formulation, we resort to some classical optics textbooks (e.g., Macleod (2010); Pedrotti, Pedrotti, and Pedrotti (2017)) and introduce some basic concepts and notation used in multi-layer thin films literature.

Each material has a property called a refractive index, which is a measure of how fast the light travels through the material. This property is important because in multi-layered applications, the effect of different refractive indices determines the reflectance of the material. Let the complex refractive index of a metallic substrate such as Tungsten s at a specific wavelength λ be denoted as $\hat{a}_s^\lambda \in \mathbb{C}$, where the imaginary part represents the reflection loss. Let \mathcal{M} represent the set of dielectric coating materials, such as Titanium Dioxide (TiO_2) and Magnesium Fluoride (MgF_2).

To quantify the reflectance of a material, we introduce the notion of transfer matrices. Transfer matrices are derived from Maxwell's equations related to the electromagnetic fields of the waves (Pedrotti, Pedrotti, and Pedrotti 2017). Assuming that the light is at normal incidence to the material, the transfer matrix of material m with thickness θ at wavelength λ is expressed as follows (here $i = \sqrt{-1}$):

$$T_m^\lambda(\theta) = \begin{bmatrix} \cos \sigma_{m,\theta}^\lambda & i \frac{\sin \sigma_{m,\theta}^\lambda}{\hat{a}_m^\lambda} \\ i \hat{a}_m^\lambda \sin \sigma_{m,\theta}^\lambda & \cos \sigma_{m,\theta}^\lambda \end{bmatrix}, \quad \sigma_{m,\theta}^\lambda = \frac{2\pi \hat{a}_m^\lambda \theta}{\lambda}. \quad (2)$$

The transfer matrices of the form (2) satisfy the following properties which will be crucial for our derivations later:

Property 1. Transfer matrices are multiplicative, meaning that the effect of coating a surface with material m_1 of thickness θ_1 , and then coating it with material m_2 of thickness θ_2 is equal to the multiplication of $T_{m_1}^\lambda(\theta_1)$ and $T_{m_2}^\lambda(\theta_2)$.

Property 2. Determinant of transfer matrices is equal to 1, i.e., $\det(T_m^\lambda(\theta)) = 1$.

Property 3. Determinant of cumulative transfer matrices is equal to 1, which is a consequence of Property 1 and Property 2.

Notice that the transfer matrices (2) have real values in the diagonal entries and imaginary values in the off-diagonal entries. For a given complex matrix $M \in \mathbb{C}^{2 \times 2}$, we denote an associated matrix $\tilde{M} \in \mathbb{R}^{2 \times 2}$ as

$$\tilde{M}_{i,j} = \begin{cases} \Re(M_{ij}) & \text{if } (i,j) \in \{(1,1), (2,2)\} \\ \Im(M_{ij}) & \text{if } (i,j) \in \{(1,2), (2,1)\} \end{cases}.$$

Since the cumulative effect of applying multiple thin films is governed by multiplication of their associated transfer matrices, the resulting multiplication is called a

cumulative transfer matrix. Now, suppose that we have a multi-layer thin film with the cumulative transfer matrix $w \in \mathbb{C}^{2 \times 2}$ coated on substrate s . Then, the reflectance of the coated material at wavelength λ is computed as

$$R_s^\lambda(w) := \frac{(\tilde{w}_{11} - \Im(\hat{a}_s^\lambda)\tilde{w}_{12} - \Re(\hat{a}_s^\lambda)\tilde{w}_{22})^2 + (\tilde{w}_{21} + \Im(\hat{a}_s^\lambda)\tilde{w}_{22} - \Re(\hat{a}_s^\lambda)\tilde{w}_{12})^2}{(\tilde{w}_{11} - \Im(\hat{a}_s^\lambda)\tilde{w}_{12} + \Re(\hat{a}_s^\lambda)\tilde{w}_{22})^2 + (\tilde{w}_{21} + \Im(\hat{a}_s^\lambda)\tilde{w}_{22} + \Re(\hat{a}_s^\lambda)\tilde{w}_{12})^2}. \quad (3)$$

To make the problem and the concepts more concrete, we provide an illustration of a two-layer thin film in Figure 1.

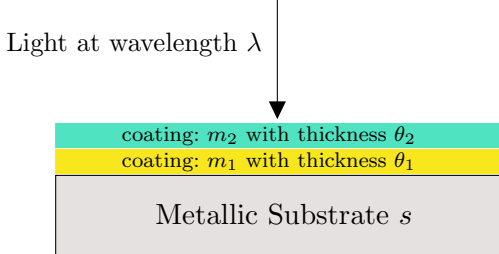


Figure 1.: Illustration of two layers of coating on top of a substrate.

Assume that on top of the metallic substrate, we coat a thin film of material m_1 with thickness θ_1 as the first layer. As the second layer, we add a thin film of material m_2 with thickness θ_2 . Then, light beams at wavelength λ are directed onto the surface and the reflectance is measured. Due to the multiplicative property, we can calculate the cumulative transfer matrix (w) in wavelength λ by multiplying the associated transfer matrices $T_{m_1}^\lambda(\theta_1)$ and $T_{m_2}^\lambda(\theta_2)$. Then, the cumulative transfer matrix can be used to calculate the reflectance of the material as in (3).

2.1. Generic Optimization Formulation

Suppose that we aim to coat a substrate s with N many thin film layers so that its reflectance is maximized for a finite set of wavelengths denoted by Λ . We would like to design a multi-layer coating that maximizes the average reflectance when the light comes at any wavelength $\lambda \in \Lambda$. Let us denote the intensity of light at wavelength λ as ϕ^λ , $\lambda \in \Lambda$. Let \mathcal{M} be the set of dielectric coating materials and Θ_m be the set of admissible thickness values for material $m \in \mathcal{M}$.

In order to formulate this situation as an optimization problem, we define decision variables μ_n and θ_n representing the material and its thickness selected for layer n , $n = 1, \dots, N$, and present the following generic formulation:

$$\max_{\mu, \theta} \left\{ \sum_{\lambda \in \Lambda} \phi^\lambda R_s^\lambda \left(\prod_{n=1}^N T_{\mu_n}^\lambda(\theta_n) \right) : \mu_n \in \mathcal{M}, \theta_n \in \Theta_{\mu_n}, n = 1, \dots, N \right\}. \quad (4)$$

Note that formulation (4) is nonlinear due to the product of matrices and the definition of the reflectance function (3), and also contains discrete decisions.

We will adapt some ideas from Kocuk (2022) to “bilinearize” and “linearize” the above formulation. Let us first define variable matrices $M_n^\lambda \in \mathbb{C}^{2 \times 2}$ and $u_n^\lambda \in \mathbb{C}^{2 \times 2}$ to represent the transfer matrix of layer n at wavelength λ and the cumulative transfer matrix up to layer n at wavelength λ , respectively. Due to Proposition 3.2 in Kocuk

(2022), $R_s^\lambda(w)$ defined in (3) can be alternatively represented as $R_s^\lambda(w) = 1 - \frac{4\Re(\hat{a}_s^\lambda)}{D_s^\lambda(w)}$, where

$$D_s^\lambda(w) := (\tilde{w}_{11} - \Im(\hat{a}_s^\lambda)\tilde{w}_{12})^2 + (\Re(\hat{a}_s^\lambda)\tilde{w}_{12})^2 + (\tilde{w}_{21} + \Im(\hat{a}_s^\lambda)\tilde{w}_{22})^2 + (\Re(\hat{a}_s^\lambda)\tilde{w}_{22})^2 + 2\Re(\hat{a}_s^\lambda). \quad (5)$$

After defining $u_0^\lambda := I$ and $w^\lambda := u_N^\lambda$ for convenience, we obtain the following formulation that is equivalent to (4):

$$\max_{\mu, \theta, M, u, w} \sum_{\lambda \in \Lambda} \phi^\lambda \left(1 - \frac{4\Re(\hat{a}_s^\lambda)}{D_s^\lambda(w^\lambda)} \right) \quad (6a)$$

$$\text{s.t. } M_n^\lambda = T_{\mu_n}^\lambda(\theta_n) \quad \lambda \in \Lambda; \mu_n \in \mathcal{M}, \theta_n \in \Theta_{\mu_n}, n = 1, \dots, N \quad (6b)$$

$$u_0^\lambda = I, u_N^\lambda = w^\lambda \quad \lambda \in \Lambda \quad (6c)$$

$$u_{n-1}^\lambda M_n^\lambda = u_n^\lambda \quad \lambda \in \Lambda, n = 1, \dots, N. \quad (6d)$$

We will specialize this formulation for the case when the applicable thicknesses for coatings are discrete sets (Θ_m is a finite set for $m \in \mathcal{M}$) and we consider maximizing the average reflectance over multiple wavelengths (i.e., $|\Lambda| > 1$).

2.2. Discrete Material Thicknesses

Assume that the thickness of each layer can be selected from a finite set Θ_m for each $m \in \mathcal{M}$. Suppose that we compute *fixed* transfer matrices $\hat{T}_{m,\theta}^\lambda := T_m^\lambda(\theta)$ a priori for each $\lambda \in \Lambda$, $m \in \mathcal{M}$ and $\theta \in \Theta_m$. We define a set of binary decision variables $x_{n,(m,\theta)}$, which take value one if layer n is coated with material m of thickness θ , and zero otherwise. Further suppose that we have polyhedral sets \mathcal{U}_n^λ , which contain all possible values of the decision variable u_n^λ , at our disposal. These polyhedral sets can be constructed using the recursive relation (6d), and they are bounded since the number of transfer matrices are finite. In order to linearize the relation (6d), we use the disjunctive formulation proposed in Kocuk (2022) by exploiting the finiteness of transfer matrices. Let us define auxiliary variables $v_{n-1,(m,\theta)}^\lambda$, which take value u_{n-1}^λ if the binary variable $x_{n,(m,\theta)}$ takes value one and zero otherwise. Then, we obtain the following equivalent optimization problem:

$$\max_{\mu, \theta, M, u, w} \sum_{\lambda \in \Lambda} \phi^\lambda \left(1 - \frac{4\Re(\hat{a}_s^\lambda)}{D_s^\lambda(w^\lambda)} \right) \quad (7a)$$

$$\text{s.t. } (6c)$$

$$\sum_{m \in \mathcal{M}} \sum_{\theta \in \Theta_m} v_{n-1,(m,\theta)}^\lambda = u_{n-1}^\lambda \quad n = 1, \dots, N \quad (7b)$$

$$v_{n-1,(m,\theta)}^\lambda \hat{T}_{m,\theta}^\lambda = u_n^\lambda \quad n = 1, \dots, N \quad (7c)$$

$$v_{n-1,(m,\theta)}^\lambda \in \mathcal{U}_{n-1}^\lambda x_{n,(m,\theta)} \quad n = 1, \dots, N, \lambda \in \Lambda, m \in \mathcal{M}, \theta \in \Theta_m \quad (7d)$$

$$\sum_{m \in \mathcal{M}} \sum_{\theta \in \Theta_m} x_{n,(m,\theta)} = 1 \quad n = 1, \dots, N \quad (7e)$$

$$x_{n,(m,\theta)} \in \{0, 1\} \quad n = 1, \dots, N, m \in \mathcal{M}, \theta \in \Theta_m. \quad (7f)$$

We can further reformulate the objective function (7a) using two more sets of auxiliary variables d_s^λ and f_s^λ satisfying the following:

$$f_s^\lambda d_s^\lambda \geq 4\Re(\hat{a}_s^\lambda) \quad \lambda \in \Lambda \quad (8a)$$

$$d_s^\lambda \leq D_s^\lambda(w^\lambda) \quad \lambda \in \Lambda \quad (8b)$$

$$f_s^\lambda \geq 0, d_s^\lambda \geq 0 \quad \lambda \in \Lambda. \quad (8c)$$

We observe that inequality (8a) is second-order cone representable, which is an important fact since it will help us build a convex relaxation of the problem later. Also, inequality (8b) is reverse convex and is the only remaining nonconvex relation (except the binary restrictions). The resulting nonconvex MIQCP is defined as below:

$$\max_{u,v,w,x,f,d} \left\{ \sum_{\lambda \in \Lambda} \phi^\lambda \left(1 - f_s^\lambda \right) : (6c), (7b) - (7f), (8) \right\}. \quad (9)$$

3. Solution Method

Two reasonable approaches appear to exist for solving the thin film spectrum optimization problem with discrete thicknesses:

- (1) MIQCP-based Approach: We solve the nonconvex MIQCP problem (9) directly using an off-the-shelf global optimization solver such as Gurobi (Gurobi Optimization, LLC 2024).
- (2) MISOCP-based Approach: We first find linear overapproximators of $D_s^\lambda(w^\lambda)$ over the variable bounds obtained from Algorithm 1 and $\det(w^\lambda) = 1$ (recall that cumulative transfer matrices have their determinant equal to one). Using these linear overapproximators, we build an MISOCP relaxation of the original nonconvex MIQCP problem as problem (12), which has a computational advantage due to its convex structure.

In the remainder of this section, we propose a bound tightening procedure that is utilized in both MIQCP and MISOCP-based methods in Section 3.1 and then develop the MISOCP formulation in Section 3.2.

3.1. *Bound Tightening*

The effectiveness of global optimization methods relies heavily on the presence of tight variable bounds, which also effect the quality of the solutions obtained by the solvers. Let us denote the lower bound and the upper bound for the (i, j) 'th entry of the variable matrices $(u_n^\lambda, n = 1, \dots, N)$, as $\underline{u}_{n,(i,j)}^\lambda$ and $\overline{u}_{n,(i,j)}^\lambda$, respectively. Then, we are able to present our bound tightening algorithm in Algorithm 1.

Algorithm 1 Bound Tightening Algorithm.

```

1: Set  $n = 1$ .
2: for all  $\lambda \in \Lambda$  do
3:   Define the set of bound matrices, initializing  $\mathcal{B}_0^\lambda = \{I\}$ .
4:   while  $n \leq N$  do
5:      $\mathcal{C}_n^\lambda = \{\}$ 
6:     for all  $\hat{T}_{m,\theta}^\lambda, m \in \mathcal{M}, \theta \in \Theta_m$  and  $B \in \mathcal{B}_{n-1}^\lambda$  do
7:        $\mathcal{C}_n^\lambda = \mathcal{C}_n^\lambda \cup \{B\hat{T}_{m,\theta}^\lambda\}$ 
8:       for all  $i \in \{1, 2\}, j \in \{1, 2\}$  do
9:         Set  $\underline{u}_{n,(i,j)}^\lambda = \min_{C \in \mathcal{C}_n^\lambda} C_{n,(ij)}^\lambda$  and  $\bar{u}_{n,(i,j)}^\lambda = \max_{C \in \mathcal{C}_n^\lambda} C_{n,(ij)}^\lambda$ .
10:        Set  $\mathcal{B}_n^\lambda := \left\{ \begin{bmatrix} u_{11} & u_{12} \\ u_{21} & u_{22} \end{bmatrix} : u_{ij} \in \{\underline{u}_{n,(i,j)}^\lambda, \bar{u}_{n,(i,j)}^\lambda\}, i \in \{1, 2\}, j \in \{1, 2\} \right\}$ .
11:       $n = n + 1$ .

```

Note that variables u_n^λ are complex numbers; we apply min and max operators separately for the real and imaginary parts of the variables in line 9 of Algorithm 1.

Recall that $u_N^\lambda = w^\lambda$ for all $\lambda \in \Lambda$. Therefore, variable bounds found after running Algorithm 1 are valid for w^λ .

3.2. Relaxation by Overapproximation of $D_s^\lambda(w^\lambda)$

Our aim is to find a linear overapproximator of the convex quadratic function $D_s^\lambda(w^\lambda)$ over the set defined by variable bounds and the constraint $\det(w^\lambda) = 1$. In order to simplify the notation, we will denote variables $\tilde{w}_{11}^\lambda, \tilde{w}_{22}^\lambda, \tilde{w}_{12}^\lambda, \tilde{w}_{21}^\lambda$ by x_1, x_2, x_3, x_4 and function $D_s^\lambda(w^\lambda)$ by $g(x)$.

Given the variable bounds, $\underline{x}, \bar{x} \in \mathbb{R}^4$ with $\underline{x} \leq \bar{x}$ and a convex function $g : \mathbb{R}^4 \rightarrow \mathbb{R}$, our aim is to find a linear overapproximator $\alpha_0 + \sum_{\ell=1}^4 \alpha_\ell x_\ell$ of $g(x)$ over $\mathcal{X} := \{x \in [\underline{x}, \bar{x}] : x_1 x_2 + x_3 x_4 = 1\}$. In other words, we aim to find $\alpha \in \mathbb{R}^5$ such that

$$\alpha_0 + \sum_{\ell=1}^4 \alpha_\ell x_\ell \geq g(x) \quad \text{for all } x \in \mathcal{X}.$$

Since g is convex, it suffices to satisfy the above condition at the extreme points of set \mathcal{X} , which are characterized as follows (Kocuk, Dey, and Sun 2018):

$$\mathcal{E} := \left(\bigcup_{\substack{\hat{x}_1 \in \{\underline{x}_1, \bar{x}_1\} \\ \hat{x}_2 \in \{\underline{x}_2, \bar{x}_2\}}} (\hat{x}_1, \hat{x}_2) \times \text{extr}(\mathcal{X}^{34}(\hat{x}_1, \hat{x}_2)) \right) \bigcup \left(\bigcup_{\substack{\hat{x}_3 \in \{\underline{x}_3, \bar{x}_3\} \\ \hat{x}_4 \in \{\underline{x}_4, \bar{x}_4\}}} \text{extr}(\mathcal{X}^{12}(\hat{x}_3, \hat{x}_4)) \times (\hat{x}_3, \hat{x}_4) \right),$$

where

$$\mathcal{X}^{12}(\hat{x}_3, \hat{x}_4) := \{(x_1, x_2) \in [\underline{x}_1, \bar{x}_1] \times [\underline{x}_2, \bar{x}_2] : x_1 x_2 = 1 - \hat{x}_3 \hat{x}_4\},$$

and

$$\mathcal{X}^{34}(\hat{x}_1, \hat{x}_2) := \{(x_3, x_4) \in [\underline{x}_3, \bar{x}_3] \times [\underline{x}_4, \bar{x}_4] : x_3 x_4 = 1 - \hat{x}_1 \hat{x}_2\}.$$

Now, we study the characteristics of sets $\mathcal{X}^{12}(\hat{x}_3, \hat{x}_4)$ and $\mathcal{X}^{34}(\hat{x}_1, \hat{x}_2)$. In general, the convex hull of a nonempty set $K := \{(y_1, y_2) \in [\underline{y}_1, \bar{y}_1] \times [\underline{y}_2, \bar{y}_2] : y_1 y_2 = \beta\}$ is one of the following types:

- Polytope: This is when variable bound constraints and constraint $y_1 y_2 = \beta$ intersects both at the negative and positive orthant. In this case, extreme points of the set $\text{conv}(K)$ consists of at most four elements given by $\{(\underline{y}_1, \beta/\underline{y}_1), (\bar{y}_1, \beta/\bar{y}_1), (\beta/\underline{y}_2, \underline{y}_2), (\beta/\bar{y}_2, \bar{y}_2)\}$.

For example, assume that the set K is characterized by $\beta = 4$ and $\underline{y}_1 = -3$, $\bar{y}_1 = 3$, $\underline{y}_2 = -2$, $\bar{y}_2 = 2$. Then, the extreme points of set $\text{conv}(K)$ (solid dots) and the set $\text{conv}(K)$ (shaded region) can be shown as in Figure 2.

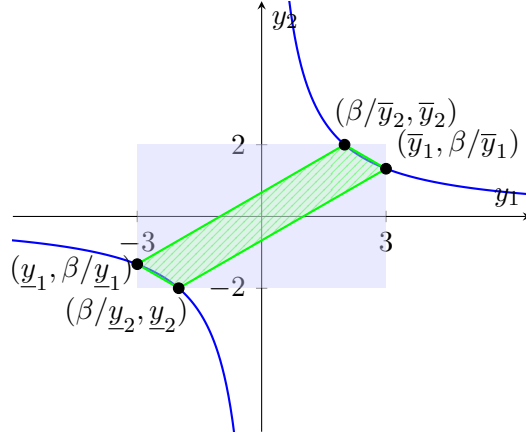


Figure 2.: An example case when $\text{conv}(K)$ is polyhedrally representable.

- Second-order cone representable: This is when variable bound constraints and $y_1 y_2 = \beta$ constraint intersect only at negative or the positive orthant. This results in a second-order cone representable set $\text{conv}(K)$. Hence, there are infinitely many extreme points in this case. However, for practical purposes, we can outer-approximate this set with a polytope and obtain its finite list of extreme points instead. For example, assume that the set K is characterized by $\beta = 4$ and $\underline{y}_1 = -1$, $\bar{y}_1 = 3$, $\underline{y}_2 = -2$, $\bar{y}_2 = 4$. Then, the points where the variable bound constraints and the constraint $y_1 y_2 = \beta$ intersect are as shown (solid dots) in Figure 3.

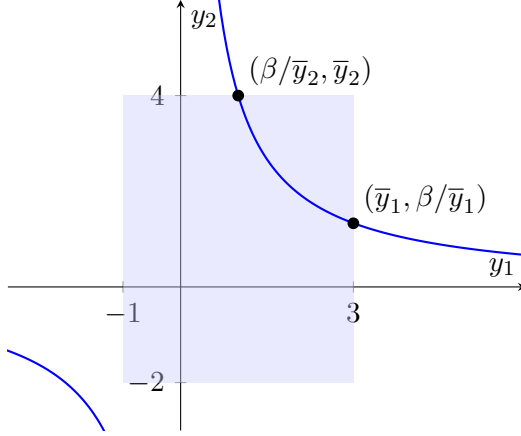


Figure 3.: An example case when $\text{conv}(K)$ is second-order cone representable.

Assume that the variable bound constraints and $y_1 y_2 = \beta$ constraint intersect at the positive orthant, i.e. $\bar{y}_1 \bar{y}_2 \geq \beta$. This is without loss of generality, since for the cases when the intersection is another orthant, we can handle it by negating the necessary variable bounds. Then, we can update the bounds we will use to outerapproximate this set as follows:

- $\underline{y}_1 = \min\{\bar{y}_1, \beta/\bar{y}_2\}$, $\bar{y}_1 = \max\{\bar{y}_1, \beta/\bar{y}_2\}$,
- $\underline{y}_2 = \min\{\beta/\bar{y}_1, \bar{y}_2\}$, $\bar{y}_2 = \max\{\beta/\bar{y}_1, \bar{y}_2\}$.

Set K consists of two points that satisfy the constraint $y_1 y_2 = \beta$ at the boundaries of the box defined by the variable bounds. To find a polyhedral outerapproximating set of K , we first calculate the geometric mean of the bounds of the first variable (denoted with filled square in Figure 4) as $(y_1, y_2) = (\sqrt{|\underline{y}_1 \bar{y}_1|}, \beta/\sqrt{|\underline{y}_1 \bar{y}_1|})$. We then draw the tangent line to the constraint $y_1 y_2 = \beta$ at that point and find the intersection points of the tangent line with the new variable bounds. Then, an outerapproximating set of $\text{conv}(K)$ is the shaded area in Figure 4.

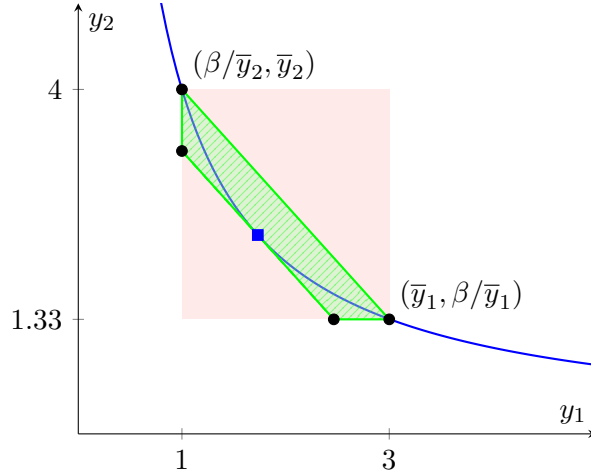


Figure 4.: Outerapproximation when $\text{conv}(K)$ second-order cone representable.

Let us denote the set of all points that are collected as $\mathcal{K} \subseteq \mathbb{R}^4$. Using these points, we aim to obtain overapproximating functions whose coefficients α satisfy

$\alpha_0 + \sum_{\ell=1}^4 \alpha_\ell x_\ell \geq g(x)$. Let us denote the set of all 5-element subsets of \mathcal{K} as $\mathcal{K}^5 := \{\mathcal{T} \subseteq \mathcal{K} : |\mathcal{T}| = 5\}$. For each subset $\mathcal{T} = \{k^{(1)}, \dots, k^{(5)}\} \in \mathcal{K}^5$, we determine the coefficients α of the affine function passing through these points by solving the following linear system:

$$\begin{bmatrix} 1 & k_1^{(1)} & k_2^{(1)} & k_3^{(1)} & k_4^{(1)} \\ 1 & k_1^{(2)} & k_2^{(2)} & k_3^{(2)} & k_4^{(2)} \\ \vdots & \vdots & \vdots & \vdots & \vdots \\ 1 & k_1^{(5)} & k_2^{(5)} & k_3^{(5)} & k_4^{(5)} \end{bmatrix} \begin{bmatrix} \alpha_0 \\ \alpha_1 \\ \alpha_2 \\ \alpha_3 \\ \alpha_4 \end{bmatrix} = \begin{bmatrix} g(k^{(1)}) \\ g(k^{(2)}) \\ g(k^{(3)}) \\ g(k^{(4)}) \\ g(k^{(5)}) \end{bmatrix}. \quad (10)$$

Then, we can find overapproximators for $D_s^\lambda(w^\lambda)$ as explained in Algorithm 2 for each wavelength λ separately to construct \mathcal{H}_λ sets.

Algorithm 2

Initialize $\mathcal{H}_\lambda = \emptyset$ (set of overapproximating functions).
for all $\mathcal{T} \in \mathcal{K}^5$ **do**
 Try to solve the linear system (10).
 Obtain the coefficient vector $\alpha \in \mathbb{R}^5$.
 if $\alpha_0 + \sum_{\ell=1}^4 \alpha_\ell k_\ell \geq g(k)$ for all $k \in \mathcal{K}$ **then**
 Add the function defined by α to \mathcal{H}_λ .

Then, we can replace constraint (8b) by the following constraint:

$$\alpha_0^{(h)} + \alpha_1^{(h)} \tilde{w}_{11}^\lambda + \alpha_2^{(h)} \tilde{w}_{22}^\lambda + \alpha_3^{(h)} \tilde{w}_{12}^\lambda + \alpha_4^{(h)} \tilde{w}_{21}^\lambda \geq d_s^\lambda \quad \lambda \in \Lambda, h \in \mathcal{H}_\lambda. \quad (11)$$

Then, we can write the MISOCP model as follows:

$$\max_{u,v,w,x,f,d} \left\{ \sum_{\lambda \in \Lambda} \phi^\lambda \left(1 - f_s^\lambda \right) : (6c), (7b) - (7f), (8a), (8c), (11) \right\}. \quad (12)$$

4. Computational Experiments

4.1. Computational Setting

We provide the results of our computational experiments in this section. We use a 64-bit workstation with two Intel(R) Xeon(R) Gold 6248R CPU (3.00GHz) processors (256 GB RAM) and the Python programming language. We utilize Gurobi 11 to solve the nonconvex MIQCPs. We set the parameter `BestObjStop` as 0.995, `MIPGap` as 0.01 and `TimeLimit` as 18000 seconds (unless otherwise stated). As the optimality gap improves very slowly over time, we focus on finding good quality feasible solutions and set the `MIPFocus` parameter as 1 and store up to 10 best solutions in the solution pool. If the solver finds an optimal solution within the time limit, it utilizes the remaining time for investigating other good quality solutions to populate the solution pool.

Following the observations from Kocuk (2022), we set the coating materials as $\mathcal{M} = \{\text{TiO}_2, \text{MgF}_2\}$. We consider Molybdenum, Niobium, Tantalum and Tungsten substrates in our study.

We carry out some preliminary experiments and observe that Titanium Dioxide (TiO_2) is used for the odd numbered layers and Magnesium Fluoride (MgF_2) for the even numbered layers in all optimal solutions. To achieve tighter variable bounds, we incorporate this information into Algorithm 1 by restricting the set of coating materials based on the layer index: specifically, $\mathcal{M}^n = \{\text{TiO}_2\}$ if n is odd and $\mathcal{M}^n = \{\text{MgF}_2\}$ if n is even.

The refractive indices that are required as an input to calculate the transfer matrices of the material-thickness pairs are obtained from Keçebaş and Şendur (2018), taken from multiple sources (Malitson 1965; Palik 1998; Dodge 1984, 1986; Golovashkin et al. 1969).

We present the reflectance profiles of the uncoated substrates in Figure 5, where the solid line represents the reflectance values in the visible spectrum (380-770 nm) while the dashed line represents the reflectance values in the broad spectrum (300-3000 nm).

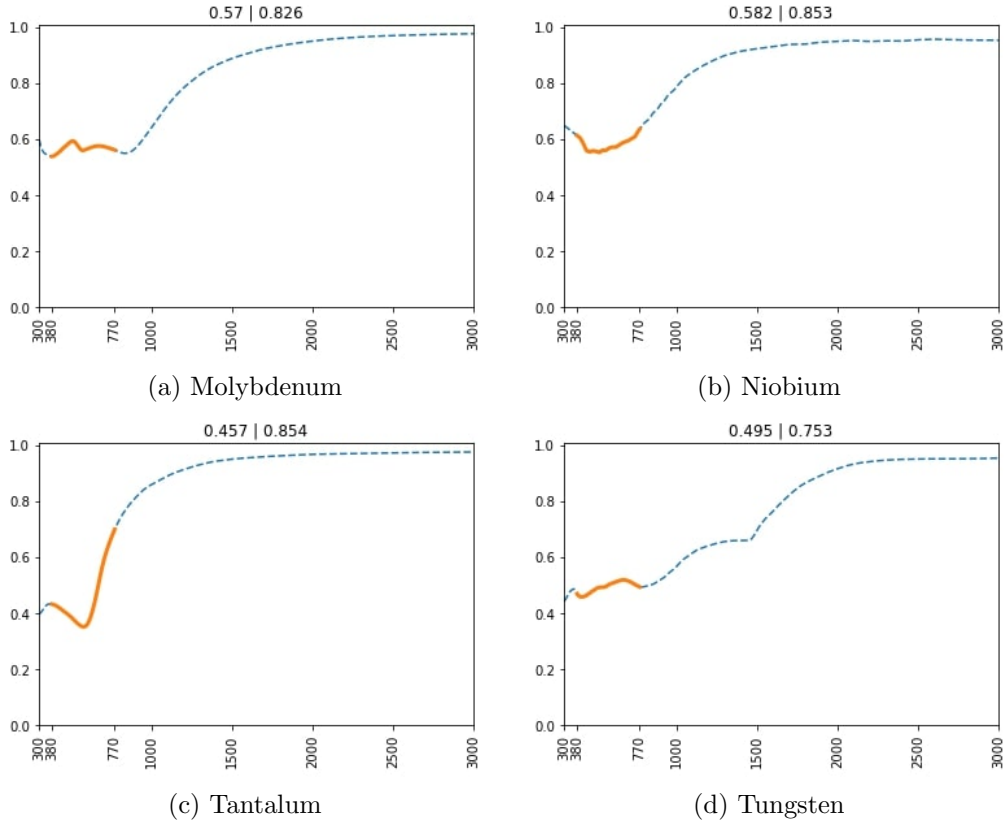


Figure 5.: Reflectance profiles of uncoated substrates.

The subfigure titles in Figures 5 and 6 present the average reflectance values calculated over the visible spectrum and the broad spectrum, respectively. For example, for the Molybdenum substrate (Figure 5a), the average reflectance for the visible spectrum and the broad spectrum are 0.570 and 0.826, respectively.

We would like to emphasize that the reported reflectance values do not correspond to the optimal objective function values. The optimization models are first solved

to obtain an optimal solution, which is then evaluated on a finer grid to assess its performance and the resulting values are reported.

4.2. Experiments for Single Wavelength

In this section, we solve the problem with MIQCP and MISOCP-based methods for some wavelengths in the visible spectrum with six layers of coating. In the experiments, the allowed thicknesses for coating are $\Theta_{\text{TiO}_2} := \{20, 30, \dots, 140\}$ and $\Theta_{\text{MgF}_2} := \{50, 60, \dots, 280\}$. Resulting reflectance values and running times in seconds are presented in Table 1 and Table 2, where ‘Refl.’ denotes the reflectance in that wavelength.

Table 1.: Comparison of MIQCP and MISOCP-based methods for Molybdenum and Niobium.

$N = 6$	Molybdenum				Niobium			
	MIQCP		MISOCP		MIQCP		MISOCP	
Wavelength(nm)	Refl.	Time	Refl.	Time	Refl.	Time	Refl.	Time
370	0.995	5.7	0.990	5.4	0.996	5.0	0.965	5.4
410	0.996	7.1	0.923	5.3	0.996	1.7	0.978	5.3
450	0.996	6.0	0.958	5.8	0.995	5.6	0.907	5.3
490	0.995	5.5	0.964	5.5	0.995	6.0	0.985	5.3
530	0.995	180.4	0.980	5.7	0.994	210.3	0.967	5.5
570	0.994	92.6	0.963	5.3	0.994	107.0	0.745	5.3
610	0.993	66.2	0.943	5.4	0.994	98.5	0.950	5.1
650	0.993	55.0	0.910	15.2	0.993	65.5	0.960	14.5
690	0.993	58.2	0.973	15.1	0.993	66.0	0.950	14.7
730	0.992	64.9	0.971	15.0	0.993	81.0	0.943	14.5
770	0.992	61.9	0.954	14.4	0.994	87.1	0.987	14.7
Average	0.994	54.9	0.957	8.9	0.994	66.7	0.940	8.7

Table 2.: Comparison of MIQCP and MISOCP-based methods for Tantalum and Tungsten.

$N = 6$	Tantalum				Tungsten			
	MIQCP		MISOCP		MIQCP		MISOCP	
Wavelength(nm)	Refl.	Time	Refl.	Time	Refl.	Time	Refl.	Time
370	0.995	5.9	0.966	5.5	0.996	6.1	0.891	5.5
410	0.996	5.5	0.973	5.6	0.996	5.7	0.973	5.5
450	0.993	160.8	0.985	5.6	0.995	151.8	0.977	5.6
490	0.992	146.1	0.930	5.4	0.994	170.4	0.967	5.3
530	0.991	155.8	0.986	5.5	0.993	178.6	0.969	5.5
570	0.989	134.9	0.844	5.5	0.993	90.2	0.964	5.3
610	0.989	98.7	0.754	5.4	0.992	65.2	0.867	5.9
650	0.991	83.8	0.797	15.1	0.992	54.6	0.904	15.0
690	0.993	77.7	0.986	14.8	0.992	60.8	0.912	15.0
730	0.994	73.8	0.964	14.7	0.991	59.4	0.927	15.1
770	0.995	5.1	0.978	14.9	0.990	67.7	0.944	15.1
Average	0.993	86.2	0.924	8.9	0.993	82.8	0.936	9.0

Examining Table 1 and Table 2, we see that by solving the MIQCP, even 6 layers of coating is sufficient to design thin films with 99% performance when we are interested in only a single wavelength. Also, solving the MISOCP is around 6 to 10 times faster than solving the MIQCP. While achieving faster solution times, the MISOCP-based method provides designs with 5 to 8% worse performance compared to the MIQCP-based method.

4.3. Experiments for the Visible Spectrum

We solve Problem (9) with its objective function discretized at different intervals and report the results in Table 3, where $\Lambda(10) := \{370, 380, \dots, 770\}$, $\Lambda(20) := \{370, 390, \dots, 770\}$ and $\Lambda(40) := \{370, 410, \dots, 770\}$. The allowed thicknesses for the coatings are the same as in Section 4.2. Then, we report the average reflectance over the visible spectrum in Table 3 and the solution times of the MIQCP problems in Table 4, where ‘TL’ denotes that the solver reached the time limit of 5 hours.

Table 3.: Average reflectance rates for the visible spectrum for the MIQCP-based method.

Substrate/ N	$\Lambda(10)$			$\Lambda(20)$			$\Lambda(40)$		
	6	10	14	6	10	14	6	10	14
Molybdenum	0.939	0.972	0.993	0.940	0.970	0.992	0.928	0.960	0.984
Niobium	0.942	0.979	0.994	0.941	0.971	0.991	0.937	0.948	0.985
Tantalum	0.931	0.976	0.991	0.927	0.977	0.991	0.916	0.961	0.979
Tungsten	0.924	0.966	0.993	0.924	0.954	0.982	0.905	0.954	0.984

Table 4.: Runtimes for the MIQCP-based method (seconds).

Substrate/ N	$\Lambda(10)$			$\Lambda(20)$			$\Lambda(40)$		
	6	10	14	6	10	14	6	10	14
Molybdenum	TL	TL	TL	TL	TL	524	TL	TL	223
Niobium	TL	TL	TL	TL	TL	TL	TL	TL	2701
Tantalum	TL	TL	TL	TL	TL	TL	TL	TL	483
Tungsten	TL	TL	TL	TL	TL	TL	TL	TL	TL

Examining Table 3, we see that the best average reflectance rates for the visible spectrum are achieved when $N = 14$ layers are coated under the objective function discretization defined by $\Lambda(10)$, the densest setting. Since the natural upper bound on the reflectance rate is 1, the results are quite satisfactory. On one hand, it is expected for the setting with $\Lambda(10)$ to perform the best since the discretization in the other settings are coarser, the optimization model does not consider the reflectance at some wavelengths. On the other hand, coarser discretization may lead to faster convergence for larger N values. For example, for $\Lambda(40)$, $N = 14$ and the substrates Tantalum, Niobium and Molybdenum, the optimization model converges within less than 45 minutes but for all other problem instances (except Molybdenum at $N = 14$ and $\Lambda(20)$, which takes around 9 minutes to solve), the solver terminates upon reaching the time limit. We present the reflectance profiles of the best solutions found by the solver in Figure 6.

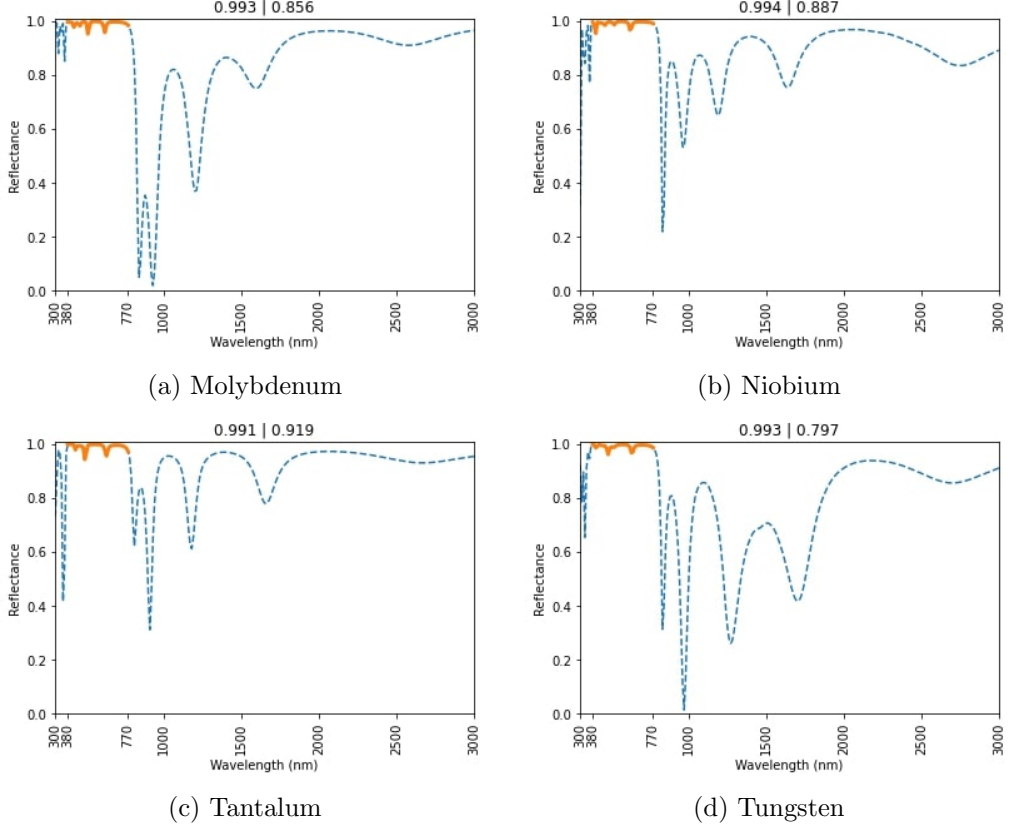


Figure 6.: Reflectance profiles with $N = 14$ layers optimized for the visible spectrum for the MIQCP-based method.

The results suggest that while 14 layers are enough to get the average reflectance rate beyond 99% for the visible spectrum, the broad spectrum performances are not satisfactory. This outcome is expected as the objective function is limited to the visible spectrum. To improve reflectance performance across a broader range, it is necessary to extend the objective function to include wavelengths beyond the visible region.

We also carry out the same experiments by utilizing the MISOCP-based method. After solving the instances with MISOCPPs with a 30-minute time limit, we evaluate their reflectance value as in Table 5 and report the time it takes to solve the MISOCP in Table 6. The results show that solving the MISOCPPs can be 10 times faster compared to solving the MIQCPs. However, solving the MISOCPPs yield on average 10.5% worse average reflectance over all instances, compared to the solutions obtained by solving the MIQCPs. The speed of the MISOCP is promising as number of coating layers increase. Therefore, it might be helpful for the broad spectrum, where we need more coating materials to achieve good reflectance values as demonstrated in Section 4.4.

Table 5.: Average reflectance rates for the visible spectrum for the MISOCP-based method.

Substrate/ N	$\Lambda(10)$			$\Lambda(20)$			$\Lambda(40)$		
	6	10	14	6	10	14	6	10	14
Molybdenum	0.796	0.892	0.915	0.783	0.847	0.911	0.814	0.884	0.864
Niobium	0.827	0.931	0.887	0.840	0.866	0.883	0.874	0.843	0.890
Tantalum	0.775	0.803	0.885	0.784	0.888	0.918	0.804	0.852	0.916
Tungsten	0.790	0.824	0.907	0.784	0.874	0.875	0.823	0.868	0.932

Table 6.: Runtimes for the MISOCP-based method (seconds).

Substrate/ N	$\Lambda(10)$			$\Lambda(20)$			$\Lambda(40)$		
	6	10	14	6	10	14	6	10	14
Molybdenum	1800	1721	1800	1800	299	703	1800	98	125
Niobium	1800	1483	1800	1800	403	325	1293	72	148
Tantalum	1800	1244	1800	169	419	518	1800	72	85
Tungsten	1800	1800	1800	237	175	624	1800	56	75

4.4. Experiments for the Broad Spectrum

To enhance the reflectance for the broad spectrum (300–3000 nm), we solve Problem (9) with different settings. We experiment with different discretizations of the objective function and material thicknesses. As observed in Figure 6, the solutions obtained by focusing on the visible spectrum exhibit high reflectance for wavelengths beyond 1500 nm, even though the optimization targets the visible range. Motivated by this observation, the setting Λ_2 considers wavelengths in the 300–1500 nm range.

In addition, we investigate two different sets of admissible material thicknesses. In the first set, thickness values are close to the quarter wavelength optical thicknesses corresponding to the visible spectrum. In the second set, thicknesses are close to the quarter wavelength optical thicknesses over the broad spectrum. The settings are specified in Tables 7 and 8.

Table 7.: Settings for objective function discretization.

Setting	Wavelengths of Light (nm)
Λ_1	$\{300, 340, \dots, 1500\} \cup \{1750, 2000, \dots, 3000\}$
Λ_2	$\{300, 340, \dots, 1460, 1500\}$

Table 8.: Settings for material thicknesses.

Setting	Coating Material	Material Thicknesses (nm)
Θ^1	MgF_2	$\{50, 60, \dots, 280\}$
	TiO_2	$\{20, 30, \dots, 140\}$
Θ^2	MgF_2	$\{50, 70, \dots, 550\}$
	TiO_2	$\{20, 40, \dots, 300\}$

Having defined the experimental setup, we are now able to present the computational results of the MIQCP-based method in Table 9, where ‘N/A’ denotes that the solver is not able to find a feasible solution within the time limit.

Table 9.: Average reflectance rates for the broad spectrum for the MIQCP-based method with $N = 20$ layers of coating.

Substrate	Setting	1-hour time limit		5-hour time limit	
		Λ_1	Λ_2	Λ_1	Λ_2
Molybdenum	Θ^1	0.915	0.941	0.942	0.951
	Θ^2	0.947	0.945	0.964	0.962
Niobium	Θ^1	N/A	0.946	0.939	0.947
	Θ^2	0.958	0.950	0.954	0.950
Tantalum	Θ^1	0.909	0.953	0.967	0.961
	Θ^2	0.955	0.954	0.966	0.966
Tungsten	Θ^1	N/A	0.909	0.943	0.949
	Θ^2	0.917	0.942	0.957	0.939

Examining the results of Table 9, we see that we are able to achieve at least 95.8% reflectance in the broad spectrum with $N = 20$ layers of coating. While the average reflectance can be further improved by increasing the number of layers, doing so makes the problem more challenging to solve. The results indicate that the setting Λ_1 with the set of material thicknesses defined by Θ^2 generally outperforms the other combinations. Therefore, we present the reflectance profiles of the setting in Figure 7.

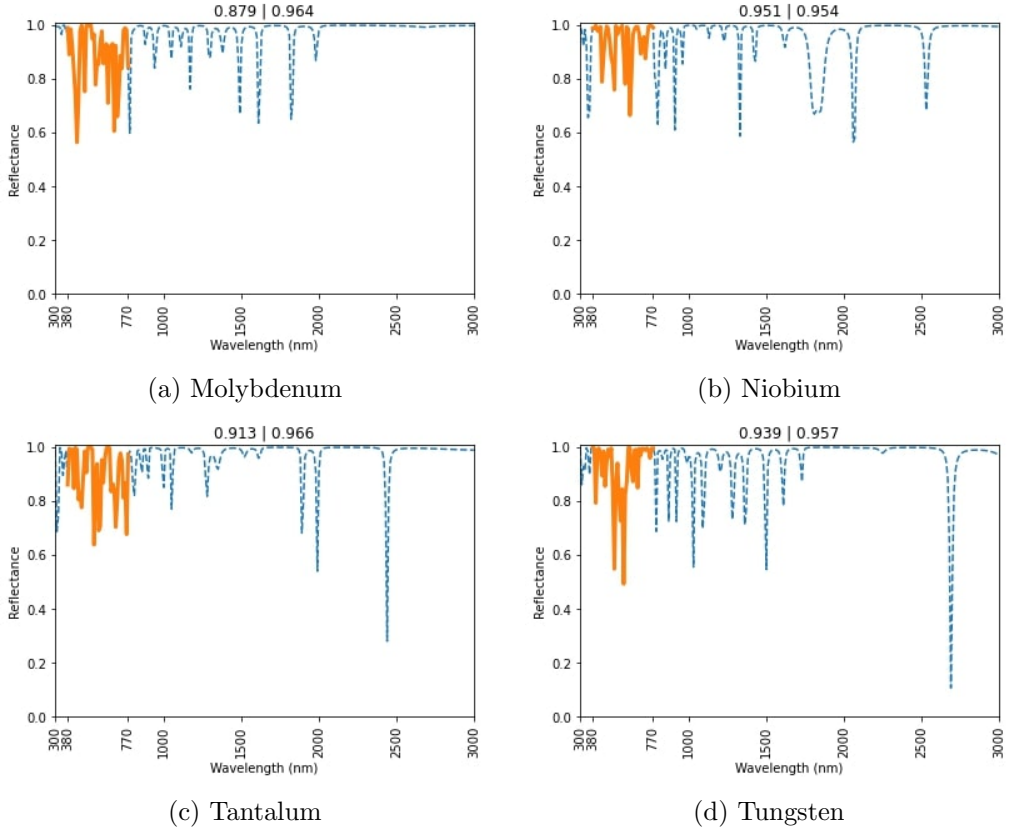


Figure 7.: Reflectance profiles with $N = 20$ layers optimized for the broad spectrum.

Examining Figure 7, we observe that when the coating design is optimized for the broad spectrum, we may see a deterioration in the reflectance for the visible

spectrum. Since the broad spectrum is much wider compared to the visible spectrum and the coating has only 20 layers, this deterioration is expected. For the Molybdenum substrate, while we are able to achieve 96.4% performance for the broad spectrum, the visible spectrum performance drops below 88%. While this trade off is natural, further improvements in reflectance across both spectra would require increasing the number of layers.

To assess the success of the proposed MISOCP-based method, we solve the MISOCP problems with a time limit of one hour. The results of the experiments are presented in Table 10.

Table 10.: Average reflectance rates for the broad spectrum for the MISOCP-based method with $N = 20$ layers of coating.

Substrate	Setting	Λ_1	Λ_2
Molybdenum	Θ^1	N/A	0.929
	Θ^2	0.893	0.919
Niobium	Θ^1	N/A	0.938
	Θ^2	0.912	0.952
Tantalum	Θ^1	0.957	0.964
	Θ^2	N/A	0.966
Tungsten	Θ^1	0.910	0.945
	Θ^2	N/A	0.943

Comparing the reflectance values reported in Table 9 and Table 10, we observe that the MISOCP-based method produces high-quality solutions. In particular, for Tantalum and Niobium substrates, the MISOCP-based approach yields solutions of nearly identical quality within one hour. The ability of the MISOCP-based method to produce high-quality solutions within reasonable computational times highlights its potential as a promising approach.

In order to demonstrate the effectiveness of the proposed methods, we compare our results with a heuristic method from the literature (Keçebaş and Şendur 2018). In this paper, the authors first specify nine wavelengths: 450, 500, 750, 900, 1000, 1200, 1500, 2000, 2200 nm. Then, for each wavelength, they design 7-layer films using the optical quarter wavelength thicknesses of the materials and then stack them on top of the substrate. Since this approach results in films with 63 layers, to obtain comparable solutions with our study, we utilize their heuristic with different number of layers. We report the average reflectance values in the broad spectrum for different number of layers in Table 11. For instance, K\$-9×2 means that 2-layer films are designed for each wavelength and then stacked, resulting in 18 layers.

Table 11.: Reflectance values of proposed methods and the heuristic.

Method- N	Molybdenum	Niobium	Tantalum	Tungsten
MIQCP-20	0.964	0.954	0.967	0.957
MISOCP-20	0.929	0.952	0.966	0.945
K\$-9×2	0.943	0.943	0.955	0.924
K\$-9×3	0.941	0.943	0.953	0.925
K\$-9×4	0.979	0.974	0.980	0.970
K\$-9×5	0.978	0.976	0.978	0.973
K\$-9×6	0.991	0.986	0.992	0.986
K\$-9×7	0.988	0.987	0.990	0.985

Examining Table 11, we observe that solving the MIQCP-based optimization model for 20 layers achieves much better reflectance values than the heuristic with 27 layers. The heuristic method surpasses the optimization based method when we allow for 36 layers to be coated, which is natural because 16 more layers are allowed to enhance the reflectance. On the other hand, MISOCP-based model also surpasses the heuristic method with 27 layers except for Molybdenum substrate, which is promising.

5. Conclusion

In this work, we develop an MIQCP-based global optimization formulation and an MISOCP-based relaxation for the Multi-Layer Thin Films Problem. We design coatings that remain effective even when the wavelength of the incident light varies. Our extensive computational experiments with the MIQCP-based method yield solutions that provide 99% reflectance in the visible spectrum and 95% reflectance in the broad spectrum. Our proposed MISOCP-based method yields competitive results with both the MIQCP-based model and a heuristic method from the literature, and is promising to yield good quality solutions as the number of coating layers increase.

There are two potential research avenues to explore: Firstly, further improvements for broad spectrum reflectance could be obtained by considering designs with a larger number of coating layers, provided that reasonable computational times can be maintained. Secondly, the tightness of the MISOCP relaxation can be enhanced and its scalability can be improved as the number of layers increases.

Disclosure statement

No potential conflict of interest was reported by the author(s).

Funding

This work was supported by the Scientific and Technological Research Council of Turkey with grant number 120C151.

Data availability statement

The data relevant to calculation of transfer matrices are obtained from Keçebaş and Sendur (2018), taken from multiple sources (Malitson 1965; Palik 1998; Dodge 1984, 1986; Golovashkin et al. 1969).

Author contributions

CRediT: **Deniz Tuncer:** Conceptualization, Data curation, Formal analysis, Investigation, Methodology, Project administration, Software, Visualization, Writing - original draft; **Burak Kocuk:** Conceptualization, Funding acquisition, Methodology, Resources, Software, Supervision, Writing - review & editing.

ORCID

Deniz Tuncer <https://orcid.org/0000-0003-0176-4937>
Burak Kocuk <https://orcid.org/0000-0002-4218-1116>

References

Azunre, Paul, Joel Jean, Carmel Rotschild, Vladimir Bulovic, Steven G Johnson, and Marc A Baldo. 2019. “Guaranteed global optimization of thin-film optical systems.” *New Journal of Physics* 21 (7): 073050. <https://doi.org/10.1088/1367-2630/ab2e19>.

Dobrowolski, J. A., Daniel Poitras, Penghui Ma, Himanshu Vakil, and Michael Acree. 2002. “Toward perfect antireflection coatings: numerical investigation.” *Appl. Opt.* 41 (16): 3075–3083. <https://opg.optica.org/ao/abstract.cfm?URI=ao-41-16-3075>.

Dodge, M. J. 1984. “Refractive properties of magnesium fluoride.” *Applied Optics* 23 (12): 1980–1985.

Dodge, M. J. 1986. “Refractive Index in Handbook of Laser Science and Technology, Volume IV.” *Optical Materials: Part 2* 2: 30.

Fouchier, M., M. Zerrad, M. Lequime, and C. Amra. 2021. “Design of multilayer optical thin-films based on light scattering properties and using deep neural networks.” *Opt. Express* 29 (20): 32627–32638. <https://opg.optica.org/oe/abstract.cfm?URI=oe-29-20-32627>.

Golovashkin, A. I., I. E. Leksina, G. P. Motulevich, and A. A. Shubin. 1969. “Optical properties of niobium.” *SOV PHYS JETP* 29 (1): 27–34.

Gurobi Optimization, LLC. 2024. “Gurobi Optimizer Reference Manual.” <https://www.gurobi.com>.

Hobson, M. P., and J. E. Baldwin. 2004. “Markov-chain Monte Carlo approach to the design of multilayer thin-film optical coatings.” *Applied Optics* 43 (13): 2651–2660.

Jiang, A., Y. Osamu, and L. Chen. 2020. “Multilayer optical thin film design with deep Q learning.” *Scientific Reports* 10 (1): 12780. <https://doi.org/10.1038/s41598-020-69754-w>.

Keçebaş, M. A., and K. Şendur. 2018. “Enhancing the spectral reflectance of refractory metals by multilayer optical thin-film coatings.” *JOSA B* 35 (8): 1845–1853.

Kim, Hansol, Mine Kaya, and Shima Hajimirza. 2021. “Broadband solar distributed Bragg reflector design using numerical optimization.” *Solar Energy* 221: 384–392. <https://www.sciencedirect.com/science/article/pii/S0038092X21003327>.

Kocuk, B. 2022. “Optimization problems involving matrix multiplication with applications in materials science and biology.” *Engineering Optimization* 54 (5): 786–804.

Kocuk, B., S. S. Dey, and X. A. Sun. 2018. “Matrix minor reformulation and SOCP-based spatial branch-and-cut method for the AC optimal power flow problem.” *Mathematical Programming Computation* 10: 557–596.

Larrauert, J. I., and R. A. M. Keski-Kuha. 1999. “Multilayer coatings with high reflectance in the extreme-ultraviolet spectral range of 50 to 121.6 nm.” *Appl. Opt.* 38 (7): 1231–1236. <https://opg.optica.org/ao/abstract.cfm?URI=ao-38-7-1231>.

Macleod, H. A. 2010. *Thin-film optical filters*. CRC press.

Malitson, I. H. 1965. “Interspecimen comparison of the refractive index of fused silica.” *Josa* 55 (10): 1205–1209.

Mashaly, Khaled. 2024. “Optimal design of multilayer optical thin film structure for smart energy saving applications using needle optimization approach.” *Physica Scripta* 99.

Palik, E. D. 1998. *Handbook of optical constants of solids*. Vol. 3. Academic press.

Pedrotti, F. L., L. M. Pedrotti, and L. S. Pedrotti. 2017. *Introduction to optics*. Cambridge University Press.

Popov, Konstantin V., J. A. Dobrowolski, Alexander V. Tikhonravov, and Brian T. Sullivan. 1997. “Broadband high-reflection multilayer coatings at oblique angles of incidence.” *Appl. Opt.* 36 (10): 2139–2151. <https://opg.optica.org/ao/abstract.cfm?URI=>

ao-36-10-2139.

Shi, Y., W. Li, A. Raman, and S. Fan. 2017. “Optimization of multilayer optical films with a memetic algorithm and mixed integer programming.” *ACS Photonics* 5 (3): 684–691.

So, Sunae, and Junsuk Rho. 2019. “Designing nanophotonic structures using conditional deep convolutional generative adversarial networks.” *Nanophotonics (Berlin, Germany)* 8 (7): 1255–1261.

Southwell, W. H. 1980. “Multilayer High Reflective Coating Designs Achieving Broadband 90° Phase Change.” In *Los Alamos Conference on Optics 1979*, edited by Donald H. Liebenberg, Vol. 0190, 81 – 88. International Society for Optics and Photonics, SPIE. <https://doi.org/10.1117/12.957727>.

Tikhonravov, A. V., M. K. Trubetskov, and G. W. DeBell. 1996. “Application of the needle optimization technique to the design of optical coatings.” *Applied Optics* 35 (28): 5493–5508.

Tran, N. M., and J. Yang. 2017. “Antibiotics Time Machines Are Hard to Build.” *Notices of the AMS* 64 (10): 1136–1140.

Turner, A. F., and P. W. Baumeister. 1966. “Multilayer Mirrors with High Reflectance Over an Extended Spectral Region.” *Appl. Opt.* 5 (1): 69–76. <https://opg.optica.org/ao/abstract.cfm?URI=ao-5-1-69>.

Wu, Z., and Q. He. 2020. “Optimal switching sequence for switched linear systems.” *SIAM Journal on Control and Optimization* 58 (2): 1183–1206.

Zhang, Kaihua, Zhiying Chen, Jinyang Guo, Shuai Gao, Kun Yu, Xiansheng Zhang, Yufang Liu, and Xiaohu Wu. 2024. “Optimization of visible transmission and NIR reflection in multilayer via PSO: Simulation and experimental validation.” *Renewable Energy* 237: 121913. <https://www.sciencedirect.com/science/article/pii/S0960148124019815>.